SYNTHESIS, CHARACTERIZATION AND APPLICATIONS OF METAL OXIDE AND MIXED METAL OXIDE NANOPARTICLES

Thesis submitted in partial fulfillment for the
Award of degree

Doctor of Philosophy

By

Ravi Kant Sharma

DEPARTMENT OF CHEMISTRY
INDIAN INSTITUTE OF TECHNOLOGY
(BANARAS HINDU UNIVERSITY)
VARANASI- 221005
INDIA

Roll No. 12611EN004

November, 2016

CHAPTER - 5

Spinel metal oxide nanoparticles

5.1. Zinc aluminate ($ZnAl_2O_4$) spinel nanoparticles

5.1.1. Introduction

Nanocrystalline zinc aluminate with spinel type structure is widely applied in various fields because of its interesting properties such as high mechanical strength, high thermal stability, low surface acidity, better diffusion, low temperature sintering ability, wide band-gap energy, hydrophobicity, excellent optical transparency, good metal dispersion capacity and chemical resistance [Zawadzki (2006), Charinpanitkul *et al.* (2009), Wei and Chen (2006), Duan *et al.* (2005)]. Nanosized zinc aluminate powders and their compact crystal structure are generally used as high temperature ceramic materials, sensors, electronic materials, catalyst and catalytic support of transition metal due to their high specific surface area [Ge *et al.* (2013), Alves *et al.* (2013), Fan *et al.* (2011)]. It has also been used as a heterogeneous catalyst in many reactions, such as acetylation, methylation, dehydration, hydrogenation, dehydrogenation and oxidation of benzyl alcohol to benzaldehyde [Ge *et al.* (2013), Fan *et al.* (2011), Farhadi and Panahandehjoo (2010), Ranjbar *et al.* (2012), Kumar *et al.* (2012)]. Zinc aluminate nanoparticles are also good photocatalysts, e.g., in the degradation of textile dye and gaseous toluene [Foletto *et al.* (2012), Li *et al.* (2011)]. Zinc aluminate ($ZnAl_2O_4$) is a typical example of normal spinel type structure having the general formula AB_2O_4, where A and B are divalent and trivalent metal ions. In this structure there are four octahedral holes and eight tetrahedral holes per molecule. In normal spinels, A^{2+} ions occupy tetrahedral holes and B^{3+} ions are

present in the octahedral holes and the anions are arranged in a cubic close packed array [Khaledi *et al.* (2012)].

$ZnAl_2O_4$ nanocrystalline powder has been synthesized by many methods such as microwave assisted hydrothermal [Zawadzki (2006)], co-precipitation [Farhadi and Panahandehjoo (2010)], hydrothermal [Yang *et al.* (2004)], solvothermal [Staszak *et al.* (2010)], combustion [Ianos *et al.* (2012)], polymeric precursors [Gama *et al.* (2009)], modified citrate [Chen *et al.* (2004)], pyrolysis [Dhak and Pramanik (2006)], microemulsion [Ciupina *et al.* (2004)], solid state high temperature reactions [Laag *et al.* (2004)] and evaporation-induced self assembly method [Tian *et al.* (2009)]. These methods need sophisticated apparatus and are expensive. The major disadvantages of the high temperature, co-precipitation and other methods are that the products obtained usually possess low surface area and inhomogeneity. The significance of the sol-gel process as compared to other methods is that it includes the ability of maintaining a high degree of purity and high homogeneity. Samples are prepared at low temperatures at low cost with good control of size, structure, and morphology [Duan *et al.* (2005), Kumar *et al.* (2012), Khaledi *et al.* (2012)]. Sol–gel method has been used to synthesize $ZnAl_2O_4$ nanoparticles by several authors. Charinpanitkul et al. (2009) and Wei and Chen (2006) have reported the preparation of $ZnAl_2O_4$ nanoparticles using ethylacetoacetate and oxalic acid as the chelating agent respectively. In the present work, very pure $ZnAl_2O_4$ nanoparticles have been synthesized without using any chelating agent.

5.1.2. Experimental

Aluminium isopropoxide (98%, ALDRICH®), zinc acetate (SRL®), toluene (RANKEM®), ammonia solution (25%, RANKEM®)), 4-nitrophenol (SRL®), $NaBH_4$ (HIMEDIA®), ethanol (MERCK®), and Millipore® water were used as the reagents as

received. In the present study, $ZnAl_2O_4$ nanoparticles were synthesized using suitable precursors by the sol-gel method. The details of procedure are as follows.

Zinc acetate : Aluminium isopropoxide (1:2 molar ratio), 100 mL of toluene, 40 mL of ethanol and 0.5 mL water (Millipore®) were taken in a 250 mL round bottom flask. The contents were vigorously stirred for 3 h at room temperature till the mixture became homogenous. Then, 2 mL of 25% ammonia solution was added followed by the addition of about 1mL of water after 1 h. The contents were kept for constant stirring for about 24 h at room temperature (25 ^oC). The obtained slurry was evaporated at 80 ^oC to form a gel. The gel was dried at ~ 80 ^oC for few hours and then grounded to obtain the xerogel powder. Then the as-prepared powder was calcined in air at 500 ^{o}, 600 ^{o} and 700 ^oC for 3 h inside a muffle furnace (Nabertherm®) to obtain $ZnAl_2O_4$ powder.

The catalytic reactivity of the synthesized nanocrystalline zinc aluminate powder was tested by carrying out the conversion of 4-nitrophenol to 4-aminophenol using $NaBH_4$ as the reducing agent at room temperature [Dhak and Pramanik (2006)]. This reaction has also been used to find the catalytic activity of different metal aluminate nanoparticles [D. Dhak and Pramanik (2006), Bayal and Jeevanandam (2012b)]. Approximately 50 mL aqueous solution of 4-nitrophenol (0.1 mmol) and 50 mL of freshly prepared aqueous solution of $NaBH_4$ (0.53 mol / L) were taken in a 250 mL beaker. Then, 18.3 mg of the catalyst (zinc aluminate nanoparticles) was added to the above mixture with constant stirring at room temperature. Complete reduction of 4-nitrophenol (yellow coloured solution) to 4-aminophenol was indicated by decolorization of the solution and the time taken for the decolorization was noted.

5.1.3. Results and Discussion

The powder XRD patterns of as-prepared and calcined zinc aluminate powder samples are shown in Figure 5.1.1. The as-prepared sample is X-ray amorphous. It is observed that

with increasing temperature crystallinity of the particles increases and also the intensity of the diffraction peaks increases showing that the particle size becomes larger. The powder sample, when calcined at 700 ^{o}C gives high intensity fine peaks. The calcined samples show peaks at 2θ ≈ 31.36 ^{o}, 36.73 ^{o}, 44.85 ^{o}, 49.09 ^{o}, 55.77 ^{o}, 59.52 ^{o}, 65.39 ^{o}, 74.19 ^{o}, and 77.35 ^{o} which are indexed as (220), (311), (400), (331), (422), (511), (440), (620), and (533) diffraction lines showing cubic crystalline zinc aluminate spinel type structure (JCPDS file no. 05- 0669). The XRD patterns confirm that the material obtained in the present work is of very high purity with single-phase. The crystallite size of pure nanocrystalline zinc aluminate was calculated using Debye-Scherrer formula. The crystallite size calculated using the most intense peak (311) at 2θ ≈ 36.73 ^{o} of nanocrystalline zinc aluminate calcined at 500 ^{o}, 600 ^{o} and 700 ^{o}C was 3.85 nm, 13.24 nm and 16.80 nm, respectively.

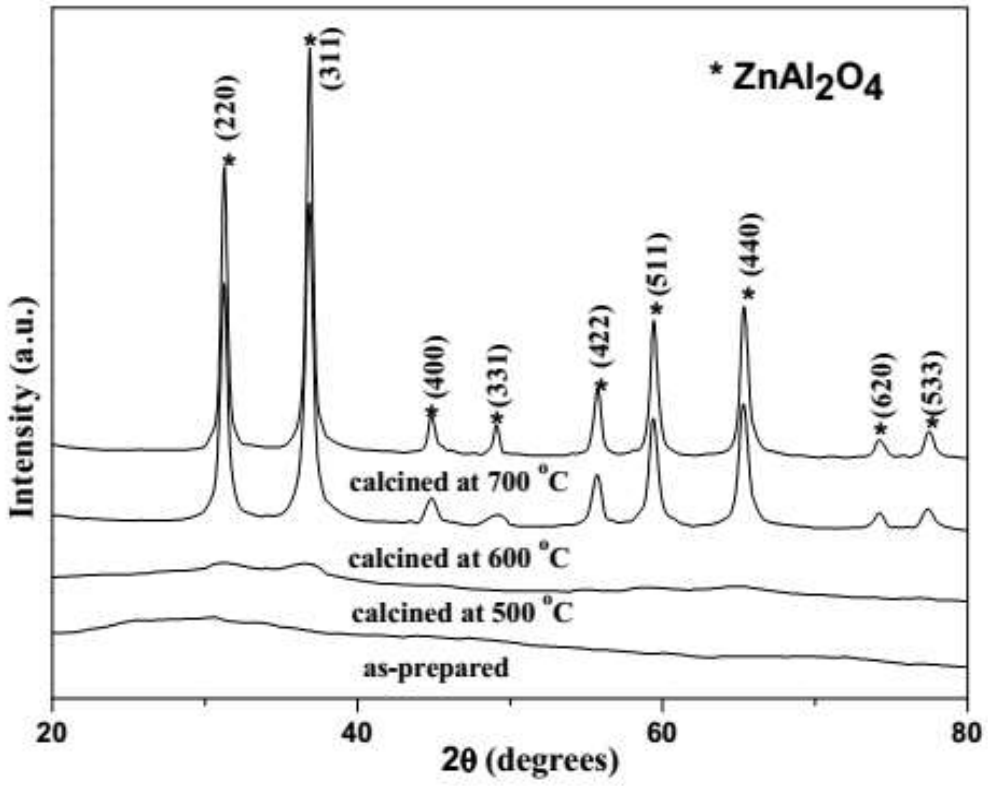

Figure 5.1.1. XRD patterns of nanocrystalline zinc aluminate (before and after calcination).

The thermal gravimetric analysis patterns for as-prepared powder show three steps of weight loss (Figure 5.1.2). The first weight loss step (9%) observed in the temperature range from 50 – 132 ^{o}C is mainly attributed to the physically adsorbed water molecules. The second weight loss (about 15 mass %) in the region 132 – 350 ^{o} C is due to the removal of organic impurities from the precursors [Ge *et al.* (2013)].

The third weight loss step in the region 350 – 500 ^{o}C is due to the decomposition of anhydrous Zn $(OH)_2 \cdot 2$ Al $(OH)_3$ to $ZnAl_2O_4$ [Farhadi and Panahandehjoo (2010)].There is no weight loss after 500 ^{o}C, confirming the formation of $ZnAl_2O_4$ spinel.

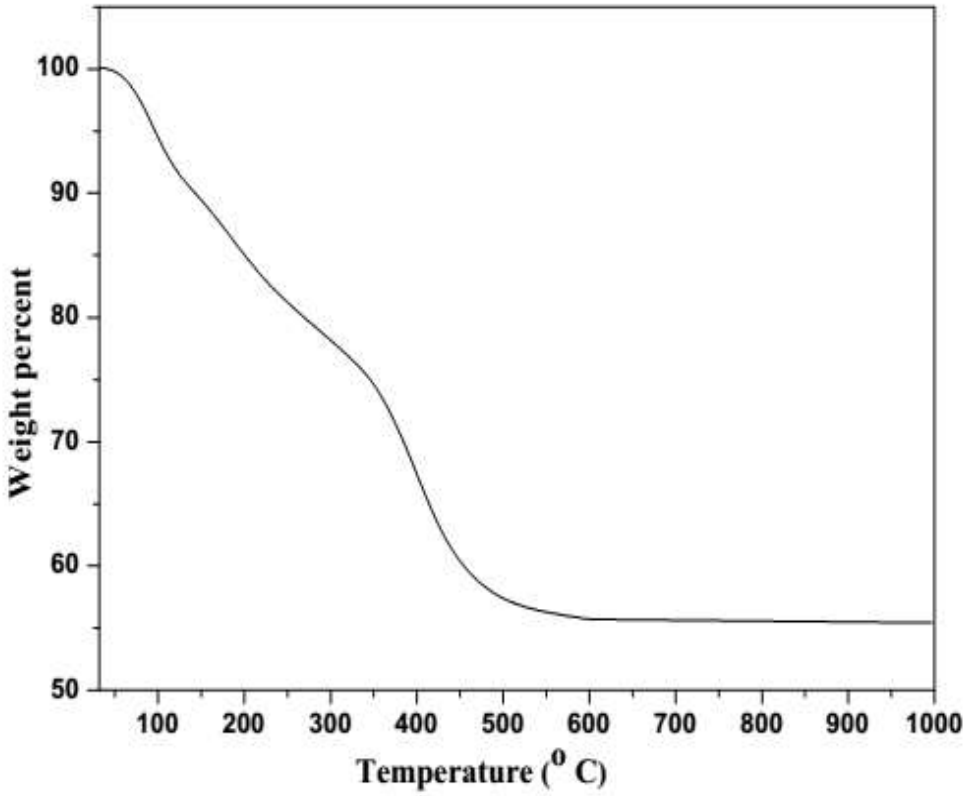

Figure 5.1.2. Thermal gravimetric analysis curves of nanocrystalline zinc aluminate.

The FT-IR spectra of as-prepared and calcined zinc aluminates show small peaks at about 2976 and 2876 cm^{-1} which attribute to C-H stretching (Figure 5.1.3) [Khaledi *et al.* (2012)]. The bands at 1727 and 1618 cm^{-1} are assigned to the free carboxyl groups [Khaledi et al. (2012)] and to the bending vibrational mode of water molecules [Staszak *et al.* (2010)] respectively.

The weak bands observed between 1572 and 1372 cm^{-1} exhibits the presence of organic compounds [Staszak *et al.* (2010)]. The bands observed between 1000-1100 cm^{-1} are assigned to the C-O and C-C vibrations [Visinescu *et al.* (2010)]. In zinc aluminate spinel powder, metal-oxygen stretching frequencies appear in the range 500-900 cm^{-1}, which is associated with the vibrations of Zn-O, Al-O, and Zn-O-Al bands [Li *et al.* (2011), Zhu *et al.* (2011)].

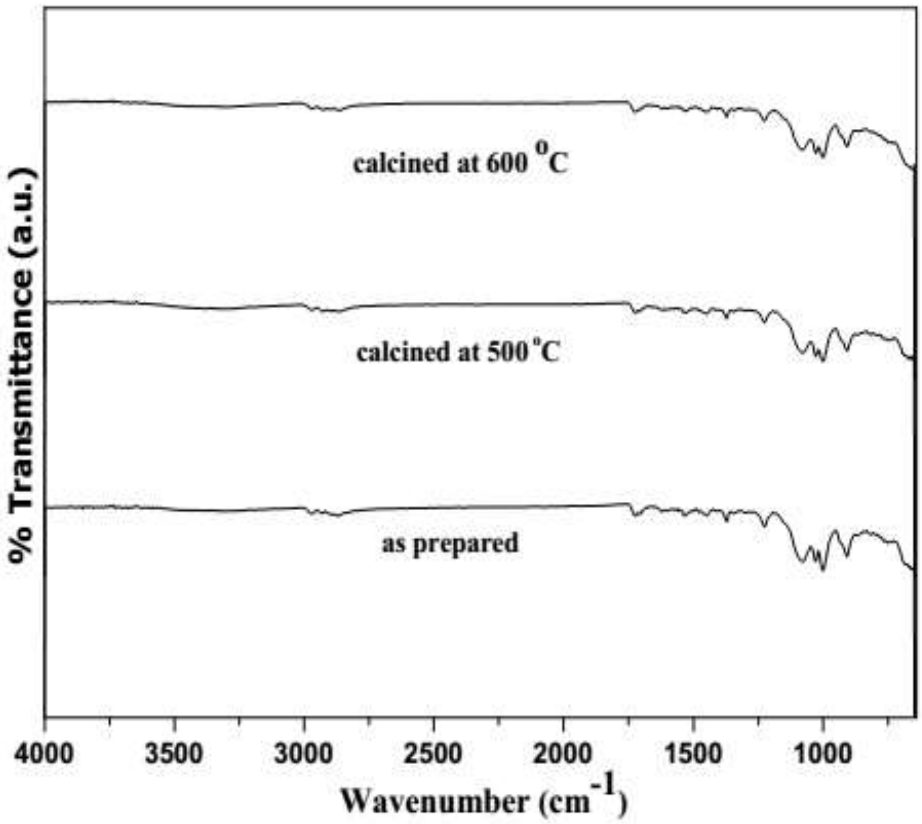

Figure 5.1.3. FT-IR spectra of nanocrystalline zinc aluminate (before and after calcination).

Diffuse reflectance spectra of nanocrystalline zinc aluminate before and after calcination at different temperatures are shown in Figure 5.1.4. The UV-visible spectra of as-prepared as well as calcined nanocrystalline zinc aluminate exhibit characteristic broad absorption band corresponding to $ZnAl_2O_4$ spinel [Kumar *et al.* (2012)].

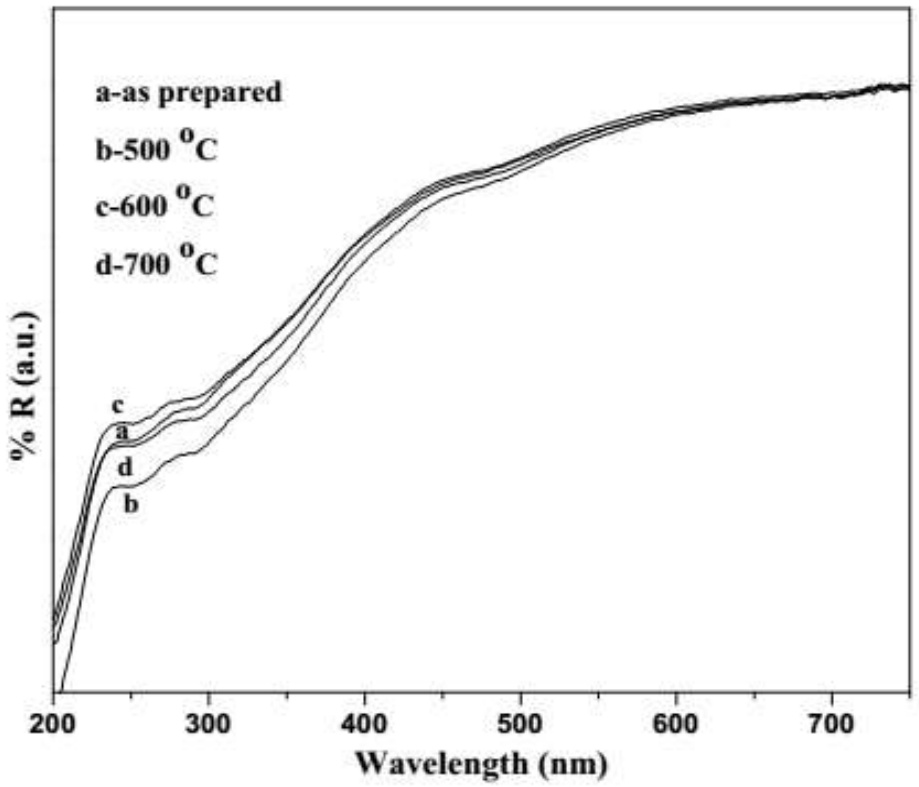

Figure 5.1.4. Diffuse reflectance spectra of nanocrystalline zinc aluminate (before and after calcination).

Surface area measurements (BET) were carried out for nanocrystalline zinc aluminate before and after calcination (Table 5.1.1). The results indicate that as-prepared zinc aluminate sample has high specific surface area (SSA ~ 332.4 m^2g^{-1}) and total pore volume (TPV ~ 0.21 cm^3 g^{-1}) compared to the calcined nanocrystalline zinc aluminate spinel (500 ^oC: SSA ~ 195.3 m^2g^{-1}, TPV ~ 0.19 cm^3 g^{-1}, 600 ^oC: SSA ~ 146.5 m^2g^{-1}, TPV~ 0.17 cm^3 g^{-1} and 700 ^oC: SSA ~129.2 m^2g^{-1}, TPV~ 0.14 cm^3 g^{-1}). Thus, $ZnAl_2O_4$ spinel powder obtained in the present synthesis method has higher surface area (given above) compared to the earlier reported methods.

The specific surface area of $ZnAl_2O_4$ spinel synthesized by the combustion [Alves *et al.* (2013)], co-precipitation [Farhadi and Panahandehjoo (2010)] and evaporation-induced self assembly [Tian *et al.* (2009)] methods are about 15 m^2g^{-1}, 86 m^2g^{-1} and 108 m^2g^{-1}, respectively.

Table 5.1.1. BET surface area and pore volume of nanocrystalline zinc aluminate before and after calcination.

Sample	Surface area (m^2 g^{-1})	Pore volume (cm^3 g^{-1})
$ZnAl_2O_4$ (before calcination)	332.4	0.21
$ZnAl_2O_4$ (calcined at 500 ^oC)	195.3	0.19
$ZnAl_2O_4$ (calcined at 600 ^oC)	146.5	0.17
$ZnAl_2O_4$ (calcined at 700 ^oC)	129.2	0.14

The FE-SEM images of the nanocrystalline zinc aluminate (before and after calcination) show agglomeration of particles with irregular morphology (Figure 5.1.5a - c).

The EDX analysis results indicate the presence of zinc, aluminium and oxygen elements in the nanocrystalline zinc aluminate powder. The atomic ratio of zinc to aluminium for the nanocrystalline zinc aluminate of as-prepared sample (i.e. at. % of Zn to Al = 1: 3) and calcined samples at 500 ^{o} and 700 ^oC (i.e. at. % of Zn to Al = 1.20: 3.40) is calculated by EDX analysis data (Table 5.1.2). The EDX analysis data indicate almost uniform distribution of zinc, aluminium and oxygen elements through the whole nanocrystalline zinc aluminate structure.

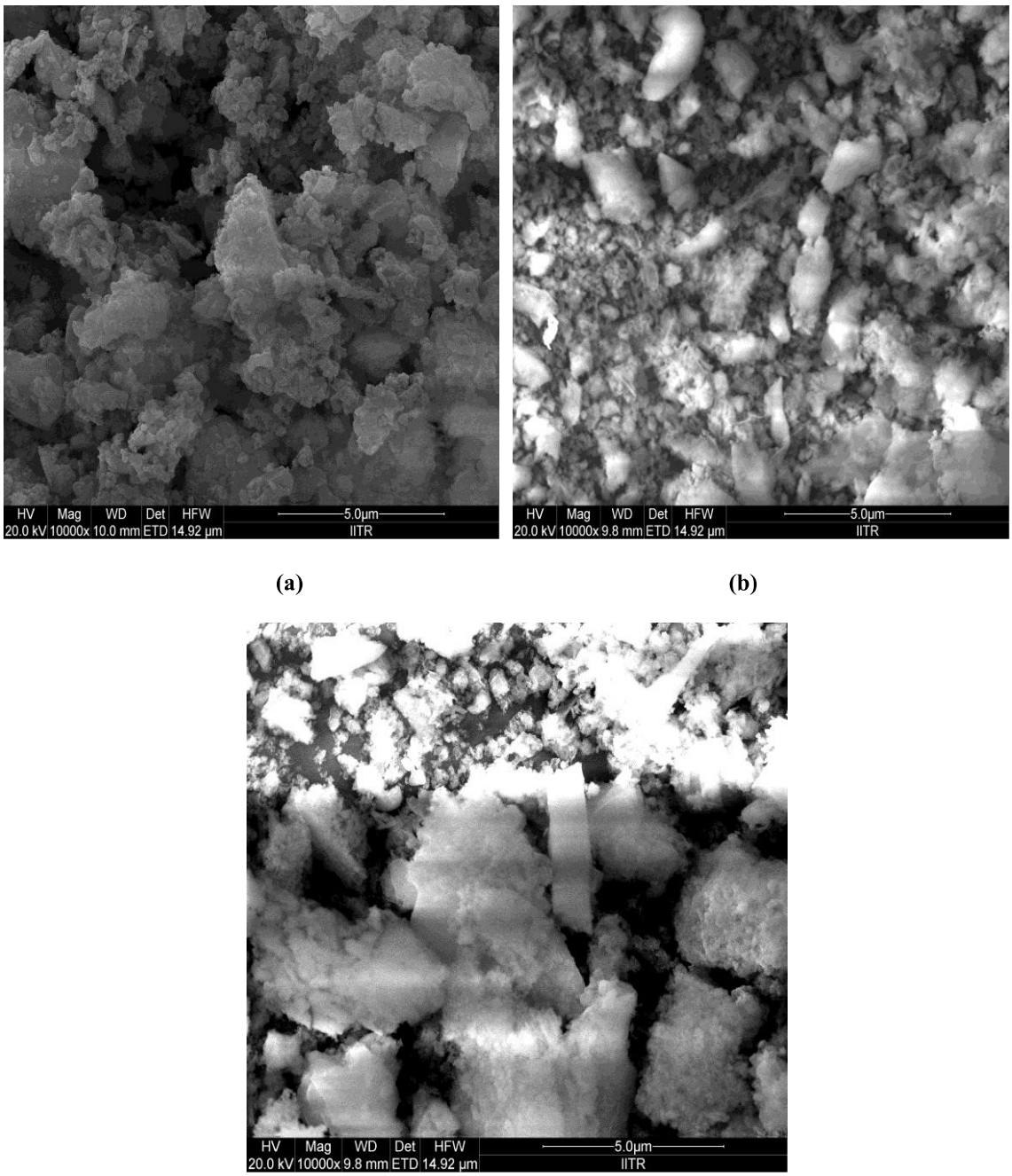

(a) **(b)**

(c)

Figure 5.1.5. SEM images of nanocrystalline zinc aluminate (a) before calcination, (b) calcined at 500 ^{o}C and (c) 600 ^{o}C.

Table 5.1.2. EDX analysis data of nanocrystalline zinc aluminate before and after calcination.

Element		At%	Wt%	Zn:Al
Nanocrystalline $ZnAl_2O_4$ before calcination	Zn	3.63	13.46	1:3
	Al	10.94	16.46	
Nanocrystalline $ZnAl_2O_4$ calcined at 500 ^{O}C	Zn	4.82	17.23	1.20:3.40
	Al	13.45	19.84	
Nanocrystalline $ZnAl_2O_4$ calcined at 700 ^{O}C	Zn	4.40	16.08	1.20:3.40
	Al	12.26	18.52	

Typical TEM images for the nanocrystalline zinc aluminate powder obtained by calcination at 500 ^{o} and 600 ^{o}C are shown in Figures 5.1.6a and 5.1.6b. The TEM images indicate that the zinc aluminate nanoparticles are close to spherical morphology with a fairly uniform distribution. The average particle size obtained from TEM images of nanocrystalline zinc aluminate calcined at 500 ^{o} and 600 ^{o}C are 6.25 ± 1.25 nm and 14.2 ± 0.96 nm, respectively. It is observed that the agglomeration of particles increases with increasing temperature.

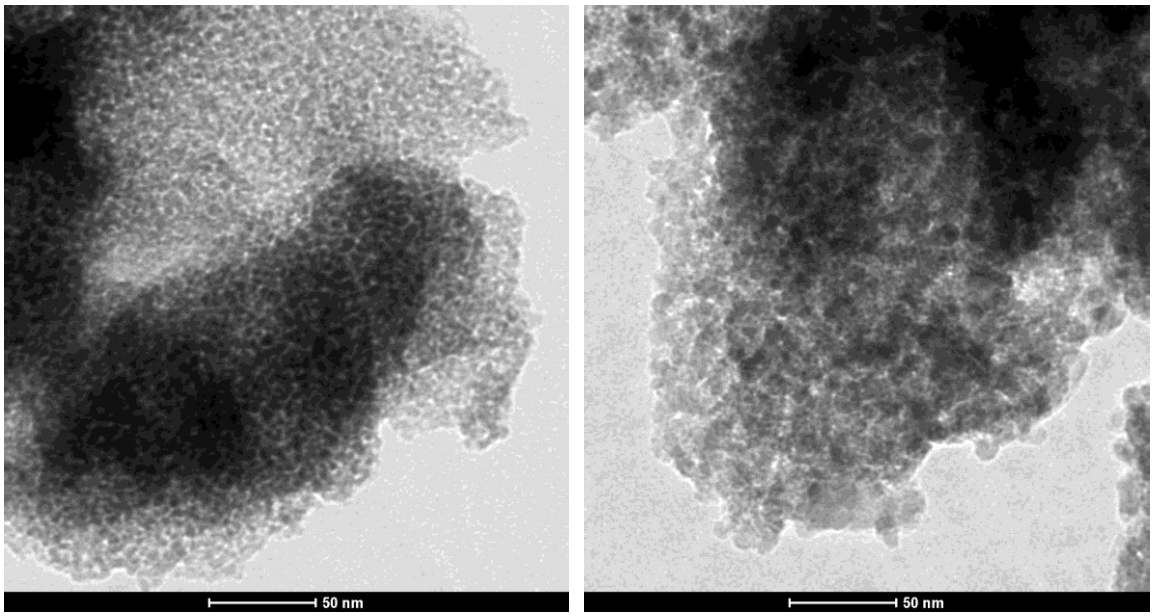

(a) **(b)**

Figure 5.1.6. TEM images of nanocrystalline zinc aluminate (a) calcined at 500 ^{o}C and (b) 600 ^{o}C.

The catalytic reactivity of the nanocrystalline zinc aluminate powder was studied using the reduction of 4-nitrophenol to 4-aminophenol by $NaBH_4$. The reduction of 4-nitrophenol with $NaBH_4$ was also carried out without the catalyst. The time required, for the complete conversion of 4-nitrophenol to 4-aminophenol, as observed by the decolorization of yellow colour of 4-nitrophenol in the presence of synthesized powders, are summarized in Table 5.1.3. From the Table 5.1.3, it is inferred that the reduction of 4-nitrophenol does not take place in the absence of the catalyst. In addition, the reduction of 4-nitrophenol does not take place when pure alumina nanoparticles are used as catalyst. The mechanism [Bayal and Jeevanandam (2012b)] for catalysis is that first the adsorption of 4-nitrophenol as well as BH_4^- ions take place on the surface of the nanocrystalline zinc aluminate powder. After that, zinc aluminate nanoparticles help in the transfer of electrons from donor BH_4^- ions to the acceptor NO_2 group and the formation of 4-aminophenolate ions take place which then get desorbed from the surface of the catalyst. The nanocrystalline zinc aluminate powder acts as a better catalyst for the reduction of 4-

nitrophenol (time of reduction: 15 min) as compared to the reported results (time of reduction: 22 min) by Dhak and pramanik (2006).

5.2. Zinc ferrite ($ZnFe_2O_4$) spinel nanoparticles

5.2.1. Introduction

Nanocrystalline spinel ferrites are of special interest due to their potential applications in various fields as in magnetic devices, catalysts, pigments, drug delivery systems and highly insulating materials [Saquib *et al.* (2013), Choudhury *et al.* (2014), Pascuta *et al.* (2011), Bardhan *et al.* (2010), Shahraki *et al.* (2012)]. Particularly Zinc ferrite ($ZnFe_2O_4$) possesses unique properties like ferromagnetism, radiation damage resistance, high thermal conductivity, mechanical hardness, excellent chemical stability, energy-transfer efficiency, high electrical resistivity, low eddy current lost and magneto-optical behavior [Naseri *et al.* (2011), Yaghmour *et al.* (2012), Lebourgeois and Coillot (2008), Hossain *et al.* (2010)]. All these properties are affected by particle size, morphology, structure, cation distributions and method of synthesis [Choudhury *et al.* (2014), Bardhan *et al.* (2010)]. It is an n-type semiconductor material with small band gap value (1.9 eV) which is used in solar cells, gas sensors, absorbent for hot gas desulphurization and also in photocatalytic applications [Tholkappiyan and Vishista (2014a), Niu *et al.* (2004), Chen *et al.* (2013), Lu and Li (1992)] due to its ability to absorb visible light with high efficiency. $ZnFe_2O_4$ nanoparticles are reported [Meidanchi *et al.* (2015)] as radiosensitizers in radiotherapy of human prostate cancer cells. The catalytic activities of $ZnFe_2O_4$ nanoparticles for O-acylation of alcohol, phenol in acetic anhydride [Moghaddam *et al.* (2012)] and in oxidative dehydrogenation of n-butene to 1, 3-butadiene [Lee *et al.* (2008)] are reported. They have been widely adopted as anode materials in commercially available lithium ion batteries [Ding *et al.* (2011)].

Bulk $ZnFe_2O_4$ has a normal spinel structure of the type $A^{2+}B_2^{3+}O_4$ where A and B refer to the metal ions at tetrahedral and octahedral sites respectively in the oxygen lattice [Grasset *et al.* (2002)]. While nanocrystalline $ZnFe_2O_4$ has a mixed spinel structure with distribution of Zn^{2+} and Fe^{3+} ions over any of the A and B-sites, which are responsible for the enhancement in magnetization compared to normal $ZnFe_2O_4$ [Atif *et al.* (2006)].

Different processes such as hydrothermal [Fan *et al.* (2009)], solvothermal [Yan *et al.* (2010)], thermal decomposition [Yang *et al.* (2013)], solid-state reaction [Shimada *et al.* (2004)], reverse micelle [Misra *et al.* (2004)], micro-emulsion [Mathew and Juang(2007)], sonochemical [Choudhury *et al.* (2013)], spray pyrolysis [Kotsikau *et al.* (2015)], combustion [Tholkappiyan and Vishista (2014b)], mechanochemical [Yang *et al.* (2004)], citrate precursor [Verma *et al.* (2005)], electrodeposition [Roy and Verma (2006)] and sol-gel [Ghasemi and Mousavinia (2014)] methods have been used to synthesize nanocrystalline $ZnFe_2O_4$. However, these techniques are difficult to develop in large-scale industrial applications because they are expensive, complicated, require sophisticated apparatus, high reaction temperatures, long production time, toxic reagents and producing by-products which are harmful to the environment. Naseri *et al.* (2011) have prepared $ZnFe_2O_4$ nanoparticles by thermal treatment method using poly (vinyl pyrrolidon) (PVP) as capping agent. Niu *et al.* (2004) have used polyoxyethylene lauryl ether, n-hexanol and n-heptance in microemulsion method. Yan *et al.* (2010) required polyethylene glycol 200 (PEG 200), teflon-lined stainless steel autoclave and longer reaction time (24 h) in solvothermal method. The surfactant oleic acid was employed by Yang *et al.* (2013) in thermal decomposition method and in the other, i.e., in mechanochemical reaction [Yang *et al.* (2004)] longer time (21 h) and high calcination temperature (600 ^oC) was needed. Shimada *et al.* (2004) have reported its synthesis by solid phase reaction at high calcination temperature (1000-1154 ^oC). Among them

homogeneous precipitation method has great scope for large scale production of nanoparticles. The advantages of this method are better control on particle size and good textural properties of the materials [Lee *et al.* (2008), Joshi *et al.* (2014), Gul et al. (2008)]. Moghaddam *et al.* (2012) employed the precipitation method for synthesis of $ZnFe_2O_4$ nanoparticles using 2.45 GHz microwave irradiation while Lee *et al.* (2008) synthesized it at high calcination temperature (650 ^oC for 6 h). In the present work the homogeneous precipitation method is adopted as it is simple and requires low calcination temperature (250 ^oC for 3h). Highly pure nanocrystalline $ZnFe_2O_4$ powders are obtained in short processing time without using any surfactant / chelating agent or special condition.

The pathogenic *Candida albicans* is the most common microorganism implicated in fungal infection [Eskandaria *et al.* (2011)]. Candidiasis is caused by overgrowth of fungal species in the genus *Candida* and it creates several types of infections in mouth, skin, blood stream, throat, intestines, heart valves and genital regions of both men and women [Molero *et al.* (1998), Berman and Sudbery (2002)]. Currently, the fungal infection candidiasis has significantly increased and in its treatment only a small number of antifungal drugs are available such as polyenes (amphotericin B), triazoles (fluconazole, itraconazole, voriconazole, posaconazole) and echinocandins (caspofungin) [Panacek *et al.* (2009)]. However, candidiasis has developed resistance, side effects, toxicity and interactions with these drugs. Hence, it is necessary to search other novel antifungal agents to avoid the above-mentioned adverse effects. This encouraged the authors to synthesize nanocrystalline $ZnFe_2O_4$ which is characterized by different techniques and its antifungal activity is explored against *Candida albicans.*

5.2.2. Experimental

(i) Materials

The chemicals Zinc acetate dihydrate (MERCK®), ferrous oxalate dihydrate (ALFA AESAR®) and ammonia solution (25%, RANKEM®) were of analytical grade and were used as reagents as received without further purification. For testing antifungal activity *Candida albicans* strain (MTCC 221) was purchased from the Culture Collection, Chandigarh, India and potato dextrose broth (PDB) medium for fungus cultures was purchased from SRL®. Millipore® water was used for the preparation of aqueous solutions.

(ii) Synthesis

In this paper nanocrystalline $ZnFe_2O_4$ spinel powders were prepared using suitable precursors by homogeneous precipitation method. The details of procedure are as follows. 80 mL aqueous solution of zinc acetate (4 mmol) and 80 mL aqueous solution of ferrous oxalate (16 mmol) were taken in a 250 mL beaker. To this mixture 15 mL of 25% ammonia solution (ammonium hydroxide) was added drop wise and the contents were heated to ~ 75 ^oC with continuous stirring for 3 h. During the reaction a dark brown precipitate formed which was centrifuged, washed with water several times to remove the impurities and further washing with ethyl alcohol dried in an oven at 80 ^oC for 8 h. The as-prepared sample was grounded to fine powder with the help of a mortar and pestle and then calcined in air at 250 ^oC and 350 ^oC for 3 h at a heating rate of 1 °C min^{-1} inside a muffle furnace. The colors of the samples before and after calcination were brown.

(iii) Antifungal activity test

The antifungal activity of the synthesized nanocrystalline $ZnFe_2O_4$ powders were tested against *Candida albicans* using disc-diffusion susceptibility method. The medium of potato dextrose broth (PDB) (~ 50 mL) was prepared by dissolving proper amount of

potato dextrose powder (39 g/L) in Millipore water and mixing it well. The final volume of 50 mL was made by further adding adequate amount of Millipore water to it. The medium was then sterilized at 121 ^{o}C ± 2 ^{o}C for 15 min and then it was kept into a sterilized petri dish for solidification. Subsequently, 50 μL of fresh suspension cultures of *Candida albicans* was evenly spread on the surface of this solidified culture medium in the petri dish with the help of a sterile glass-rod spreader. The petri dish was left standing for 15 minutes so that the culture got absorbed in the medium. Then a sterilized filter paper disc (8 mm diameter) was placed at the centre of the petri dish. 10 mg/mL of the nanocrystalline $ZnFe_2O_4$ powders were mixed with sterilized Millipore water with the help of a low power sonicator. This was then impregnated onto the filter paper disc of the petri dish. After 4 days of incubation of this petri dish in a thermostatic chamber at 27 ^{o}C a clear zone of inhibition was observed around the disc. The antifungal activity was investigated by measuring the diameter of this zone of inhibition in millimetre (mm). The experiments were repeated several times to minimize experimental error and the mean value of these diameters is reported.

5.2.3. Results and discussion

Appropriate amount of ammonium hydroxide solution was added to a mixture of aqueous zinc acetate and aqueous ferrous oxalate with continuous stirring for 3 h at about 75 ^{o} C and the following reactions take place:

$$2Zn(CH_3COO)_2 \bullet 2H_2O\ (aq.) + 4FeC_2O_4 \bullet 2H_2O\ (aq.) + 12NH_4OH\ (aq.) \rightarrow$$
$$ZnFe_2O_4 + Zn(OH)_2 + 2FeO(OH) + 4CH_3COONH_4 + 4(NH_4)_2C_2O_4 +$$
$$2H_2O + 2H_2\ (g) \qquad (5.2.1)$$

Also after calcination process:

$$Zn(OH)_2 + 2FeO(OH) \rightarrow ZnFe_2O_4 + 2H_2O \qquad (5.2.2)$$

Pure $ZnFe_2O_4$ powders are formed after calcination which is confirmed from the XRD data.

The X-ray powder diffraction patterns of as-prepared and calcined samples (at 250 ^oC and 350 ^oC) are reported in Figure 5.2.1. The XRD pattern of the as-prepared sample shows three phases: one due to iron oxide hydroxide FeO(OH) (JCPDS file no. 22-0353), second due to orthorhombic phase of $Zn(OH)_2$ (JCPDS file no. 89-0138) and the third for $ZnFe_2O_4$ (JCPDS file no. 22-1012). The diffraction peaks of 2θ values are observed at 29.9^o, 35.3^o, 42.8^o, 53.3^o, 56.8^o, and 62.3^o for the samples calcined at 250 ^oC and 350 ^oC. These peaks are indexed to the (220), (311), (400), (422), (511), and (440) reflection planes respectively corresponding to face-centered cubic spinel structure of $ZnFe_2O_4$ with lattice parameter of a = 0.8441 nm (space group: Fd3m, Z = 8; JCPDS file no. 22-1012). These results indicate that after calcination iron oxide hydroxide FeO(OH) and $Zn(OH)_2$ reacts to form highly pure face-centered cubic spinel structure of $ZnFe_2O_4$. The crystallite sizes of the nanocrystalline $ZnFe_2O_4$ are determined from the most intense peak at (311) plane of the X-ray diffraction data using the Debye–Scherrer formula. The crystallite sizes of the nanocrystalline $ZnFe_2O_4$ calcined at 250 ^oC and 350 ^oC are found to be 2.9 and 4.3 nm respectively.

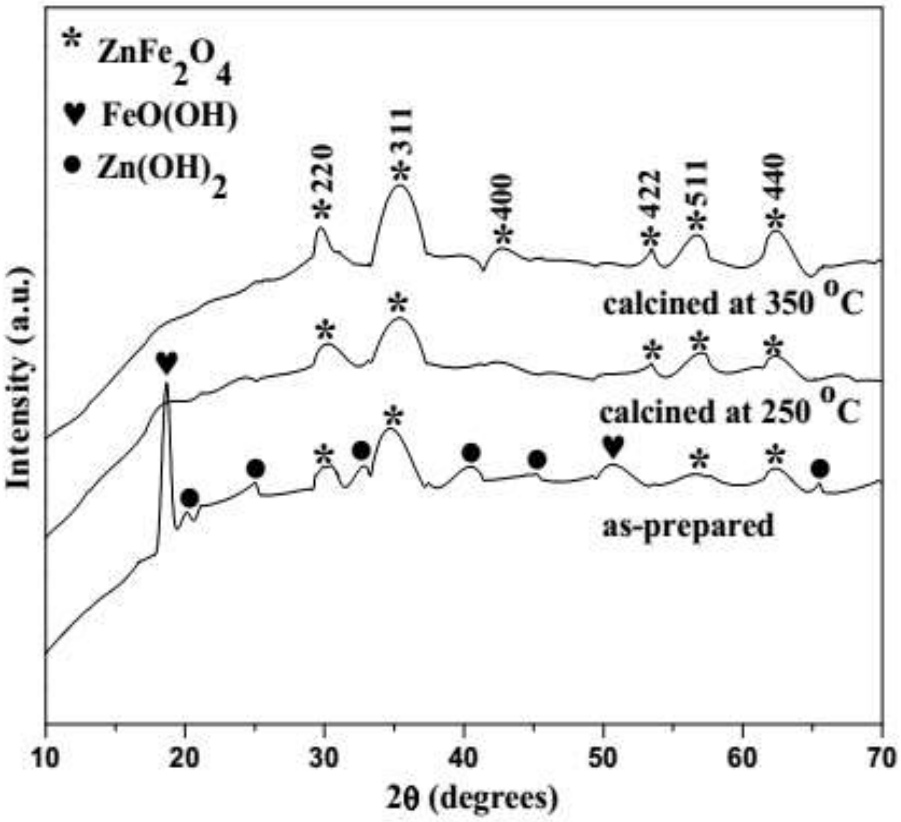

Figure 5.2.1. XRD patterns of as-prepared and calcined samples at 250 ^{o} and 350 ^{o}C.

The thermal gravimetric analysis curve of the as-prepared sample shows weight loss of about 28 % in the region 39–250 ^{o}C that is attributed to the release of water molecules from the reaction between FeO(OH) and $Zn(OH)_2$ (Figure 5.2.2). There is no weight loss after 250 ^{o}C confirming the formation of pure nanocrystalline $ZnFe_2O_4$.

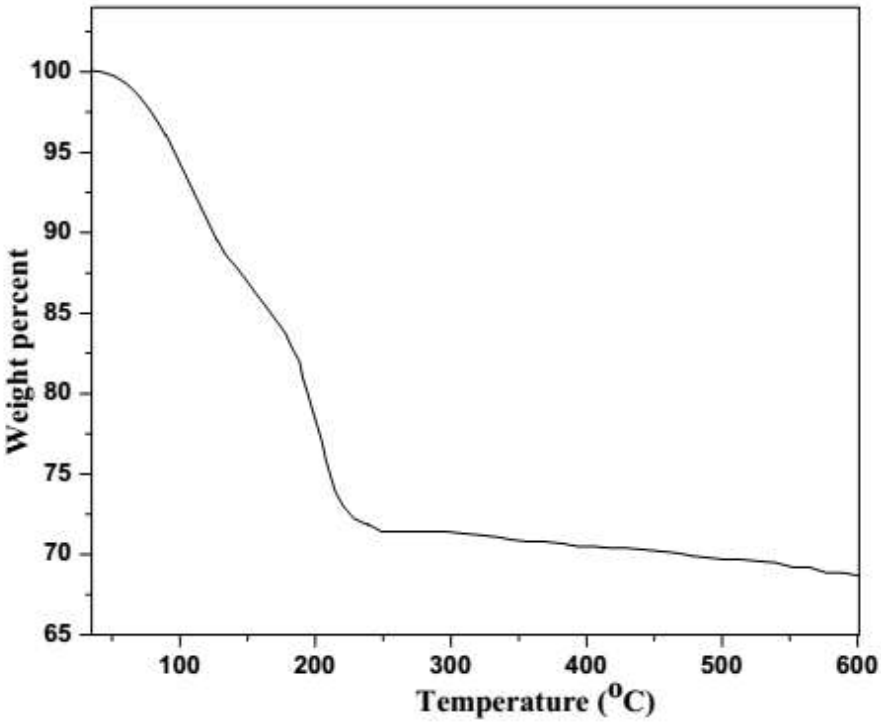

Figure 5.2.2. Thermal gravimetric analysis curves of as-prepared sample.

The FT-IR spectra of the as-prepared and calcined samples are shown in Figure 5.2.3. The broad band observed in the region 3363 cm^{-1} corresponds to O–H stretching vibrations arising from the moisture present in KBr which is used for making pellets in an open air. The band at 1653 cm^{-1} present in the spectrum of the as-prepared sample is assigned to bending vibrations of water molecules [Darezereshki *et al.* (2011)]. In the spectrum of the as-prepared sample the band at 1322 cm^{-1} is attributed to the symmetric C=O bond vibrations. The band at about 833 cm^{-1} in the as-prepared sample is due to Fe-OH bond vibrations [Ghasemi and Mousavinia (2014)]. The peak appearing in the region of 669 cm^{-1} is due to the presence of hydroxyl group in the as-prepared sample [Thangaraj *et al.* (2011)]. In the FT-IR spectra of all spinels and ferrites two characteristic metal-oxygen absorption bands appear in particular [Moghaddam *et al.* (2012)]. The peaks with wavenumbers 563 and 436 cm^{-1} are assigned to the stretching vibrations of Zn–O bonds in tetrahedral positions and Fe–O bonds in octahedral positions respectively [Meidanchi *et al.* (2015), Moghaddam *et al.* (2012)].

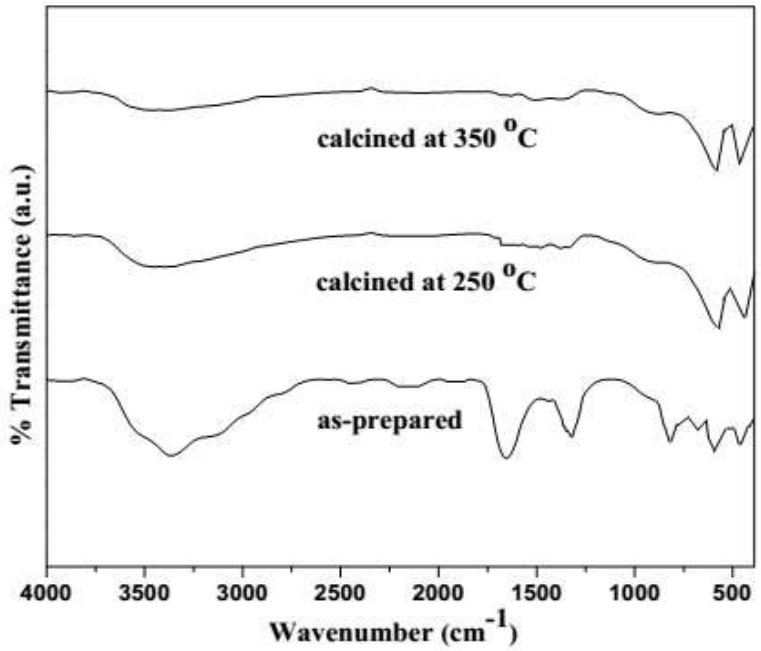

Figure 5.2.3. FT-IR spectra of as-prepared and calcined samples at 250 ^{o} and 350 ^{o}C.

UV–visible diffuse reflectance spectroscopy is one of the significant methods to reveal the band structure or molecular energy levels in the materials. Diffuse reflectance spectra of nanocrystalline $ZnFe_2O_4$ powders calcined at 250 ^{o}C and 350 ^{o}C are shown in Figure 5.2.4 (a). These show that the nanocrystalline $ZnFe_2O_4$ powders absorb significant amount of visible light in the range 200–540 nm. The absorption in the visible region by the ferrite is attributed to electron excitation from the O-2p level into the Fe-3d level which is observed for the spinel-type compound [Su *et al.* (2012)]. Kubelka-Munk function [Fan *et al.* (2009)] is used to calculate the optical absorption coefficient (α):

$$\alpha = (1\text{-}R)^2/2R \qquad (5.2.3)$$

where R is the diffuse reflectance. The optical band gap (Eg) of the nanocrystalline $ZnFe_2O_4$ is determined from the absorption coefficient (α) using the Tauc relation [Tholkappiyan and Vishista (2014a)]:

$$(\alpha h\upsilon)^n = K(h\upsilon - E_g) \qquad (5.2.4)$$

where hυ is the energy of the incident photon, K is the constant related to the material and n depends on the nature of band transition, i.e., n = 2 for allowed indirect and n = 1/2 for

allowed direct transitions [Kislov *et al.* (2008)]. The $(\alpha h\upsilon)^2$ on the y axis versus energy of exciting light ($h\upsilon$) on the x-axis is plotted in Figure 5.2.4(b) on the basis of data obtained from Figure 5.2.4(a). The energy band gap estimated from the UV–visible spectra of nanocrystalline $ZnFe_2O_4$ is ~ 2.30 eV [Tholkappiyan and Vishista (2014a), Fan *et al.* (2009)].

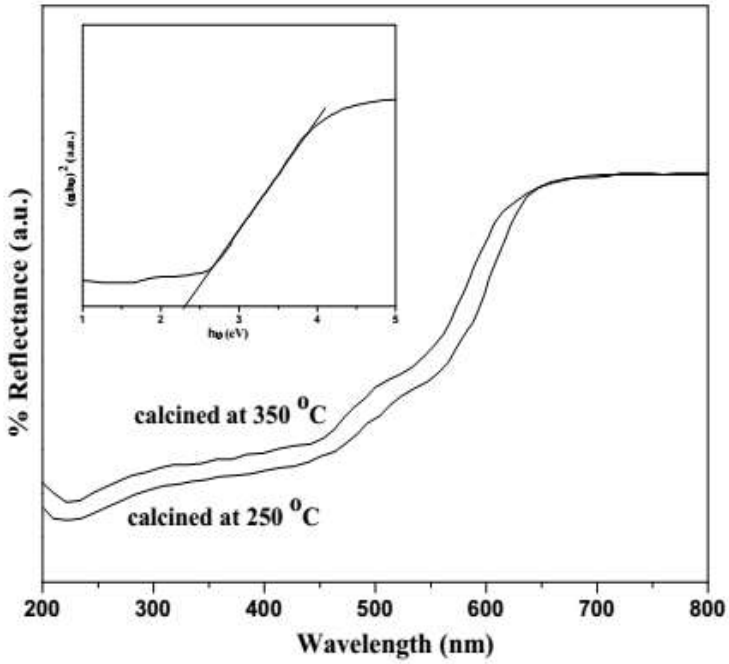

Figure 5.2.4. (a) Diffuse reflectance spectra of nanocrystalline $ZnFe_2O_4$ spinel, and (b) The plot of $(\alpha h\upsilon)^2$ vs. $h\upsilon$ according to the data from (a).

BET (Brunauer-Emmett-Teller) surface area measurements were carried out for the as-prepared and calcined samples. The specific surface area and total pore volume for these samples are represented in Table 5.2.1. The results indicate that the nanocrystalline $ZnFe_2O_4$ calcined at 250 ^oC possesses high specific surface area (~ 152.3 m^2g^{-1}) and total pore volume (~ 0.14 $cm^3\ g^{-1}$) compared to those of as-prepared (SSA ~ 137.8 m^2g^{-1} and TPV ~ 0.11 $cm^3\ g^{-1}$) and sample calcined at 350 ^oC (SSA ~ 143.6 m^2g^{-1} and TPV ~ 0.12 $cm^3\ g^{-1}$). The specific surface area of the nanocrystalline $ZnFe_2O_4$ synthesized in the present work is significantly higher than those obtained by co-precipitation [Lee *et al.* (2008)], water-in-oil microemulsion [Grasset *et al.* (2002)], colloid mill-hydrothermal

[Fan *et al.* (2009)] and high-energy ball milling [Kislov *et al.* (2008)] methods, which are about 31.3 m^2g^{-1}, 12 m^2g^{-1}, 100.5 m^2g^{-1} and 37.18 m^2g^{-1}, respectively.

Table 5.2.1. BET surface area and pore volume of the samples before and after calcination.

Sample	Surface area (m^2 g^{-1})	Pore volume (cm^3 g^{-1})
As-prepared powder	137.8	0.11
$ZnFe_2O_4$ calcined at 250 ^oC	152.3	0.14
$ZnFe_2O_4$ calcined at 350 ^oC	143.6	0.12

Agglomeration of small spherical-like particles is observed in the FE-SEM images of the as-prepared and calcined samples (Figure 5.2.5(a)–(c)). The energy dispersive X-ray (EDX) spectrum indicates the presence of Zn, Fe and O elements in the synthesized nanocrystalline $ZnFe_2O_4$ sample (Figure 5.2.5d). The EDX analysis data of the samples give the atomic ratio of Zn to Fe in the as-prepared sample as 0.48 while in the calcined samples at 250 ^oC and 350 ^oC as 0.49 and 0.50, respectively (Table 5.2.2). The EDX analysis data confirmed the presence of highly pure and almost uniform distribution of Zn, Fe and O elements in the nanocrystalline $ZnFe_2O_4$ samples.

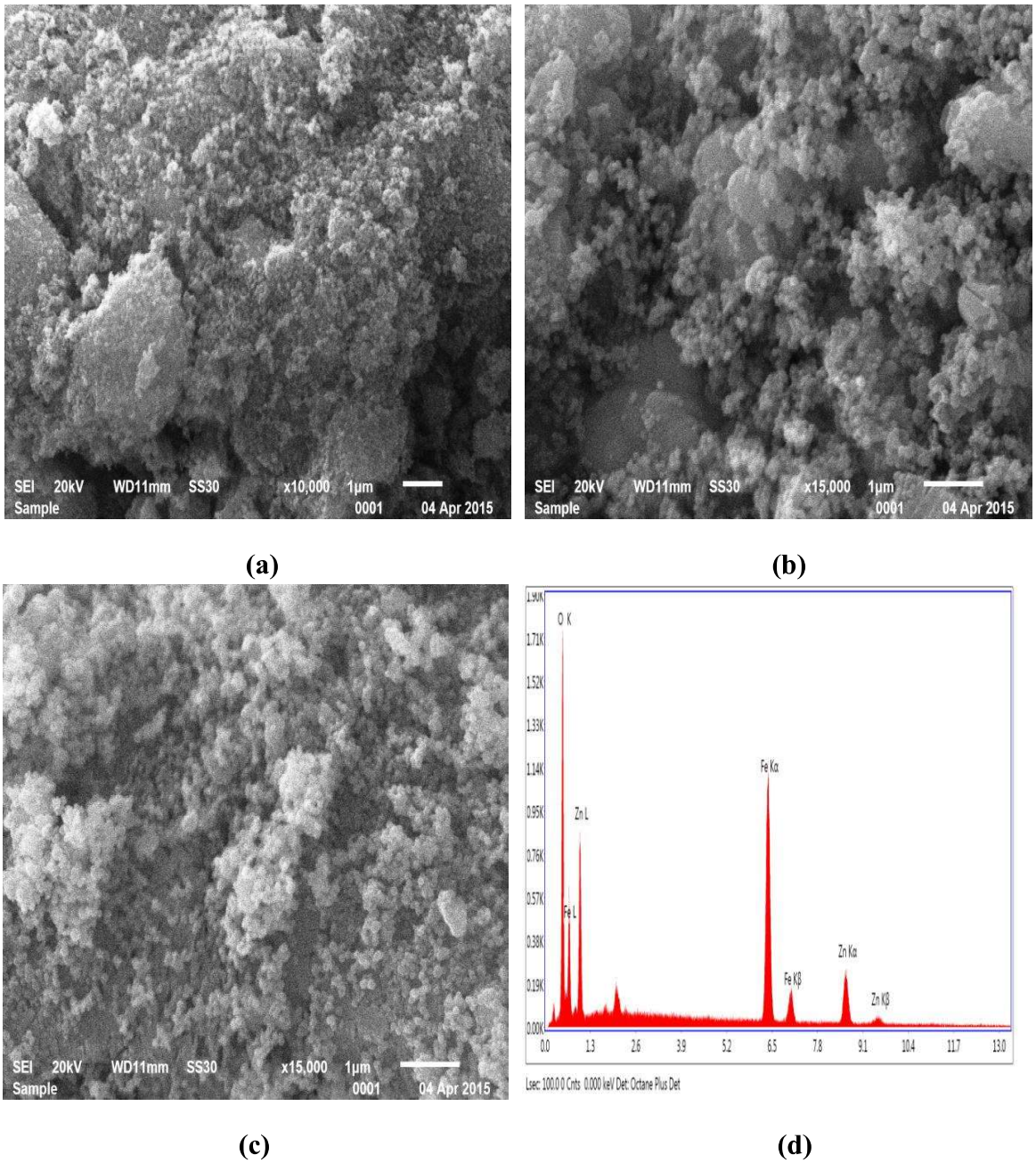

Figure 5.2.5. FE-SEM images of samples (a) as-prepared, (b) calcined at 250 ^{o}C, (c) calcined at 350 ^{o}C, and (d) EDX analysis plot of nanocrystalline $ZnFe_2O_4$.

TEM image of the sample after calcination at 350 ^{o}C is shown in Figure 5.2.6(a). It is observed that the nanocrystalline $ZnFe_2O_4$ obtained on calcination at 350 ^{o}C exhibits spherical particles with almost uniform distribution. The average particle size of nanocrystalline $ZnFe_2O_4$ estimated from TEM measurement is 5.2 ± 0.61 nm which is in accordance with the results of powder X-ray diffraction analysis.

The selected-area electron diffraction (SAED) pattern of the nanocrystalline $ZnFe_2O_4$ is shown in Figure 5.2.6(b). The ring SAED pattern is related to the diffraction from the single phase zinc ferrite with nanocrystalline structure which is consistent with the XRD results.

Table 5.2.2. EDXA data of as-prepared and calcined samples.

Sample	Element	At%	Wt%	Zn/Fe
As-prepared powder	Zn	13.23	25.82	0.48
	Fe	27.44	45.78	
	O	59.33	28.36	
$ZnFe_2O_4$ calcined at 250 ^oC	Zn	15.35	27.84	0.49
	Fe	31.28	48.43	
	O	53.37	23.68	
$ZnFe_2O_4$ calcined at 350 ^oC	Zn	17.74	29.78	0.50
	Fe	35.31	50.73	
	O	46.95	19.37	

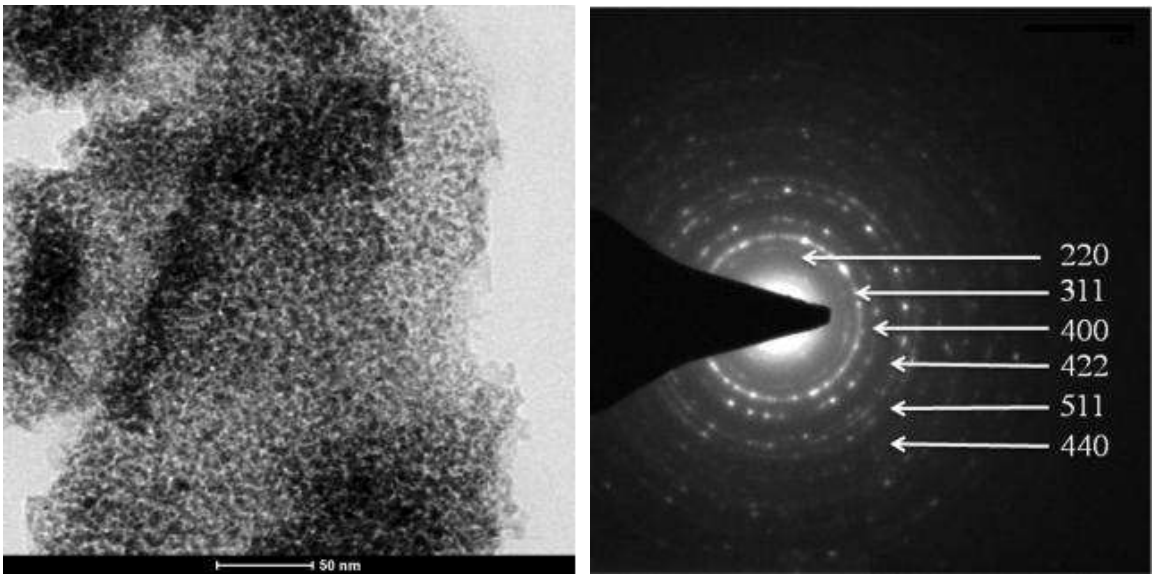

Figure 5.2.6. (a) TEM image and (b) corresponding SAED pattern of nanocrystalline $ZnFe_2O_4$.

The antifungal activity test of nanocrystalline $ZnFe_2O_4$ powders was carried out against pathogenic *Candida albicans* by disc diffusion susceptibility method (Figure 5.2.7). The result indicates the diameter of the zone of inhibition around the disc to be 12.5 ± 0.3 mm in the presence of nanocrystalline $ZnFe_2O_4$ (10 mg/mL). The production of ROS such as hydrogen peroxide, superoxide anion, hydroxyl radical, and hydroxyl ion by nanocrystalline $ZnFe_2O_4$ are responsible for its antifungal activity [Pasquet *et al.* (2014), Rasmussen *et al.* (2010), Shoeb *et al.* (2013)]. The mechanism of the generation of ROS from nanocrystalline $ZnFe_2O_4$ is due to its semiconductor properties. The presence of large numbers of valence band holes and/or conduction band electrons in nanocrystalline $ZnFe_2O_4$ are the main cause for its redox reactions even in the absence of UV light. The size of nanocrystalline $ZnFe_2O_4$ is very small and this decreases its nanocrystal quality by increasing the interstitial zinc ions, iron ions, oxygen vacancies along with donor/acceptor impurities. Thus a large number of electron-hole pairs (e^- + h^+) are formed in the system. Holes being powerful oxidizing agents decompose water molecules derived from the environment of aqueous $ZnFe_2O_4$ into H^+ and OH^-. The conduction band electrons are good reducing agents, they move to the nanoparticle surface to react with dissolved oxygen molecules and thus superoxide radical anions ($O_2^{\bullet-}$) are generated. This $O_2^{\bullet-}$ radical anions react with H^+ producing $HO_2^{\bullet}$ radicals. The $HO_2^{\bullet}$ radicals further combine with electrons forming hydrogen peroxide anions (HO_2^-). These HO_2^- anions interact with hydrogen ions finally generating hydrogen peroxide (H_2O_2). The ROS thus produced rupture the fungal cell membrane decreasing its fungal enzymatic activity. The penetration of generated H_2O_2 into the cell membrane helps to kill the fungi. The negatively charged particles like hydroxyl radicals and superoxides remain on the outer surface of the membrane. The nanocrystalline $ZnFe_2O_4$ possesses a large surface-to-volume ratio and this plays the significant role for its stronger antifungal activity.

Figure 5.2.7. Antifungal activity of 10 mg/mL concentration of nanocrystalline $ZnFe_2O_4$ tested against pathogenic *Candida albicans.*

5.3. Conclusions

Single-phase nanocrystalline zinc aluminate ($ZnAl_2O_4$) spinel powder has been synthesized by sol-gel method without using any chelating agent. Zinc aluminate nanoparticles were formed at 600 ^oC, which is at much lower temperature than by solid state reactions. Formation of $ZnAl_2O_4$ and their particle size depend on the calcination temperature. Calcination temperature also affects the specific surface area, pore volume and surface morphology. The nanocrystalline powder was characterized using various analytical techniques. Surface area measurements indicate that nanocrystalline zinc aluminate obtained under sol-gel method has high surface area. Catalytic activity of the nanocrystalline zinc aluminate powder was tested for the reduction of 4-nitrophenol to 4-aminophenol. The studies indicate that the present nanocrystalline powder acts as a better catalyst compared to earlier reported work.

Single-phase nanocrystalline zinc ferrite ($ZnFe_2O_4$) spinel powders have been successfully synthesized by an easy homogeneous precipitation method in short

precipitation time at low calcination temperature (250 ^{o}C). The samples have been characterized using different analytical techniques. Nanocrystalline $ZnFe_2O_4$ obtained in the present work is spherical in shape and has high surface area with small particle size. The antifungal activity of the nanocrystalline $ZnFe_2O_4$ was tested against pathogenic *Candida albicans* by disc diffusion susceptibility method. It is observed that the present nanocrystalline powders exhibit excellent antifungal behavior for the pathogenic *Candida albicans*. In future, the antifungal activity study of the nanocrystalline $ZnFe_2O_4$ will be extended to other microbial strains.